SYNTHESIS AND CHARACTERIZATION OF $SrCo_2O_4$ IMMOBILIZED ON MODIFIED CLAY WITH ENHANCED REMOVAL OF CONGO RED FROM AQUEOUS MEDIUM

OUARDIA SEBBAH [a], LAMIA BENNABI [b], HADJ BENHEBAL [c,], SAMIR KADI [d], JULIEN G MAHY [e], AND STÉPHANIE D LAMBERT [e]*

[a]*Synthesis and Catalysis Laboratory/ Ibn Khaldoun University Tiaret, Tiaret (14000) Algeria.*
[b]*Faculty of Technological Sciences / University Belhadj Bouchaib of Ain Temouchent , Algeria.*
[c]*Department of Chemistry, Faculty of Matter Sciences, Ibn Khaldoun University Tiaret, Tiaret (14000) Algeria.*
[d]*Laboratory of Plant physiology Applied to Above-Soil Culture, Department of Nature and Life Sciences, Ibn Khaldoun University Tiaret, Tiaret (14000) Algeria.*
[e]*Department of Chemical Engineering–Nanomaterials, Catalysis and Electrochemistry, B6a, University of Liege, 4000 Liege, Belgium.*

ABSTRACT

Photocatalysis is an efficient and cost-effective method for removing toxic dyes from wastewater. Indeed, a large part of the research work carried out in the field of green chemistry has been devoted to the design and development of new photocatalysts with good photocatalytic activities. Incorporation of supports constitutes a strategy to improve the photocatalytic activity of photocatalysts by reducing the aggregation of nanoparticles during the photocatalytic process. Intercalated clays can be used as supports for oxide-based photocatalysts because they have high adsorption capacity. The goal of the present study consists of using $SrCo_2O_4$ nanoparticles as photocatalyst immobilized on natural Algerian clay modified by polyaniline (Clay/PANI/$SrCo_2O_4$). Spinel oxide ($SrCo_2O_4$) was synthesized through a sol–gel method. Then, polymer modified clay were fabricated by in situ polymerization. The as-prepared composites were characterized by powder X-ray diffraction (XRD), Fourier transform infrared spectrophotometry (FTIR) and Scanning electron microscopy (SEM). The photocatalytic performances of the synthesized materials were evaluated by studying the photocatalytic degradation of congo red dye under UV light irradiation.

Keywords: *Photocatalysis, Composite, Clay, Polyaniline, $SrCo_2O_4$, Congo Red.*

1. INTRODUCTION

Clean drinking water has become increasingly scarce in the majority of countries due to excessive consumption on the one hand and its pollution on the other. Thus the resources available for our daily consumption and to meet our numerous demands are reduced. A wide range of contaminants responsible for water pollution can be classified into several categories: organic, inorganic, heavy metal ions, radioelements, pathogenic microorganisms and so on[1]. Featuring physicochemical stability, high molecular weight and complex structure, organic pollutants such as dyes, pharmaceuticals, phenols, pesticides, fertilizers, surfactants, etc., are not biodegradable and will persist in water for a long time [2]. Highly toxic even at low doses, the chemical dyes released in large quantities by different industrial sectors into the environment can cause numerous diseases in humans such as; skin irritations, allergic dermatitis and cancers [3-6.]. Recent studies estimate that approximately 7×10^7 tons of synthetic dyes are produced worldwide each year, of which 15,000 tons are discharged into wastewater [7,8]. Congo red is an anionic benzidine-based azo, water-soluble dye [9]. Its metabolism into the carcinogenic product "benzidine" can cause skin, eye and gastrointestinal irritation [10,11]. There are a variety of physical and chemical pollutant removal processes from polluted water such as precipitation, adsorption, flocculation, reverse osmosis and ultra-filtration [12]. Despite the efforts made to improve these processes, most of them remain incapable of being totally effective because many chemical dyes are based on aromatic or heterocyclic ring structures, which are considered non-biodegradable non-biodegradable and relatively stable [13,14]. With very few limitations in terms of efficiency, advanced oxidation processes (AOP) present themselves as the most appropriate techniques for the treatment of water soluble organic dyes [15,16]. Among advanced oxidation processes, heterogeneous photocatalysis takes pride of place as a powerful water treatment technology that has attracted the interest of researchers due to its ability to completely mineralize target pollutants [17]. But achieving an efficient application of photocatalytic technology requires a better choice and good exploitation of photocatalysts [18]. The application of metal oxide semiconductors as photocatalysts critically depends on their properties such as bandgap structure, light absorption range, morphology, average crystallite size, specific surface area and chemical stability [19]. Due to the wide bandgap of conventional photocatalysts such as e.g. TiO_2, ZnO, WO_3, the application of photocatalysis under visible radiation for water treatment remains ineffective. For this reason, many researchers have focused on the development of new reduced bandgap materials with a low charge recombination rate and high visible light absorption capacity. There are some bimetallic spinel oxides with properties that can be useful as photocatalysts for the water treatment by photocatalysis. Cobalt based spinel oxides with general formula A(II)Co_2O_4 (while A (II) = Zn, Ni, Cu, Mn, Fe,…..) exhibit magnificent catalytic activity caused by the availability of more active sites [20-27]. Clays are very important versatile materials that can be used in many fields due to their exceptional physicochemical properties. These include low cost, wide availability, chemical inertness, excellent adsorption capacity, cation exchange capacity, strong surface reactivity and good mechanical and thermal stability [28-30]. Clay minerals and their modified forms have attracted particular attention due to their use in the field of water treatment as adsorbents, photocatalytic materials and photocatalyst carriers. Clays as photocatalyst carriers can both inhibit the agglomeration of photocatalyst nanoparticles and reduce photogenerated charge recombination [31]. Additionally, clays can accelerate the photocatalytic reaction due to the presence of numerous adsorption and activation sites on their surface due to the interfacial contact between photocatalysts and organic pollutant [32-33]. However, the adsorption capacity of clay minerals in the raw state is limited and in order to overcome this problem, functionalization by organic intercalation remains necessary [34]. Organically intercalated clays are synthesized by the insertion of organic molecules inside in their interlayer space, resulting in an increase in basal spacing. They constitute a very attractive class of 2-dimensional microporous materials for the adsorption of various organic molecules [35,36]. In this experimental work, clay material with porous structure was intercalated by in-situ intercalative polymerization of polyaniline to form a support for attachment of cubic spinel $SrCo_2O_4$ nanoparticles used as a photocatalyst for the degradation of congo red in aqueous medium. To the best of our knowledge there are no studies related to the synthesis, characterization and applications of $SrCo_2O_4$.

2. EXPERIMENTAL PART

2.1. Materials and reagents

The reagents used in this work were of analytical quality and were used without prior treatment: Cobalt nitrate ($Co(NO_3)_2.6H_2O$; Merck. Darmstadt), Strontium nitrate ($Sr(NO_3)_2$, Merck Darnstadt), Citric acid ($HOC(COOH)(CH_2COOH)_2$; Biochem Chemopharma.), Ethanol (CH_3CH_2OH; VWR Chemicals), Aniline ($C_6H_5NH_2$; GPR Rectapur), Iron(III) chloride ($FeCl_3$; Sigma-Aldrich), Hydrochloric acid (HCl; Sigma Aldrich) and Clay extracted from Tiaret, west Algeria.

2.2. Preparation

a) **$SrCo_2O_4$ synthesis:** the spinel oxide strontium cobaltite ($SrCo_2O_4$) nanoparticles were synthesized by sol-gel process using the metal nitrate $Co(NO_3)_2.6H_2O$ and $Sr(NO_3)_2$ as precursors, citric acid as chelating agent, ethanol as solvent. In a typical experiment (figure-1.a), appropriate amounts of $Sr(NO_3)_2$ (1.423g) and $Co(NO_3)_2\cdot6H_2O$ (4.713g) were

**Corresponding author email: benhebal@univ-tiaret.dz*

separately dissolved in ethanol (Sr:Co molar ratio of 1:2). After complete dissolution, the two solutions were mixed then stirred for 15 minutes. A bright pink solution was obtained. Also, anhydrous citric acid was dissolved in distilled water to form another solution. Solution of citric acid was slowly dripped into the previous mixture. Citric acid to metal ratio in mixtures was of 2:1. Then the solution obtained was heated under continuous stirring at 70°C to evaporate solvent until viscous liquid was formed. The gel is dried in an oven then ground into a fine powder and finally calcined at 600°C in an oven.

b) ***Composite preparation:*** As presented in figure-1.b, the Clay/PANI/$SrCo_2O_4$ nanocomposite was prepared by in situ oxidative chemical polymerization of aniline monomer in an acidic medium in the presence of pure clay and $SrCo_2O_4$ nanoparticles powder (Clay:PANI: $SrCo_2O_4$ molar ratio of 1:2:1) [37]. Initially 0.2 g $SrCo_2O_4$ nanoparticles and 0.2 g clay were dispersed in 15 ml HCl(1M) and maintained in an ultrasonic bath for 3 hours at 30°C, then 0.4 ml aniline were added to the previous mixture and kept under ultrasonic for 2 hours at the same temperature. The resulting homogeneous suspension was then transferred into a round bottomed flask placed in an ice bath, then polymerization was initiated by adding dropwise 15 mL of HCl (1M) containing $FeCl_3$ (0,5 g) and the reaction was kept under magnetic stirring for 24 hours at 5°C to complete the polymerization process. After the time had elapsed, the resulting precipitate was separated from the solution by centrifugation, washed with HCl (0.1 M) followed by distilled water and ethanol. Finally, the resulting product was vacuum dried at 60°C, and ground to a fine powder of Clay/PANI/$SrCo_2O_4$ nanocomposite.

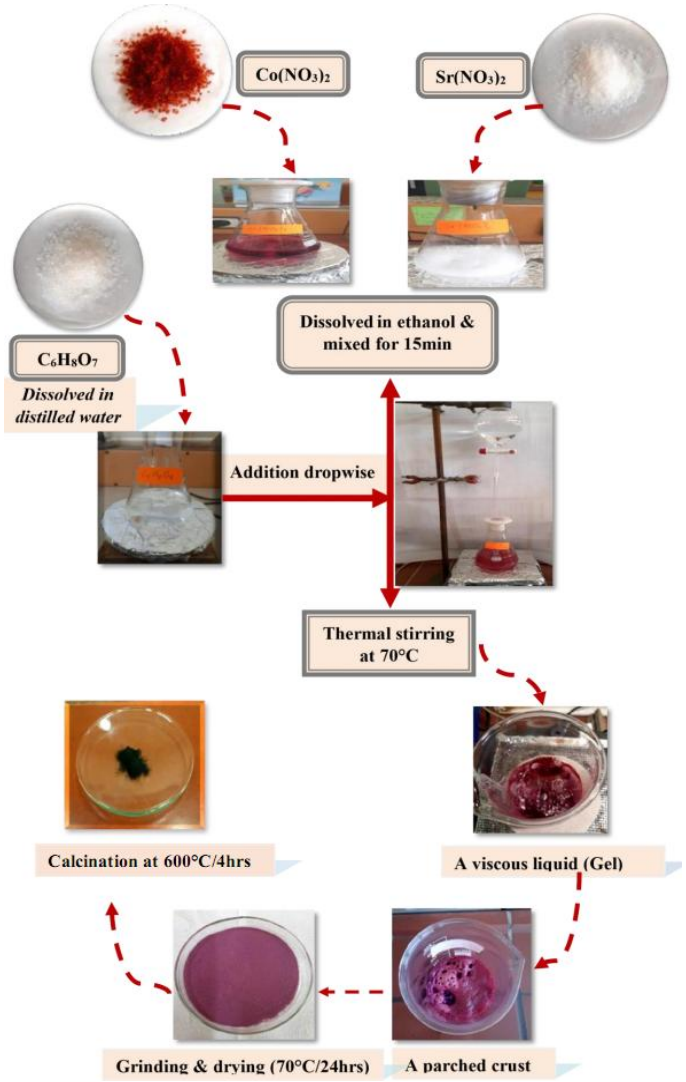

Figure 1.a: Flowchart of $SrCo_2O_4$ nanoparticle preparation

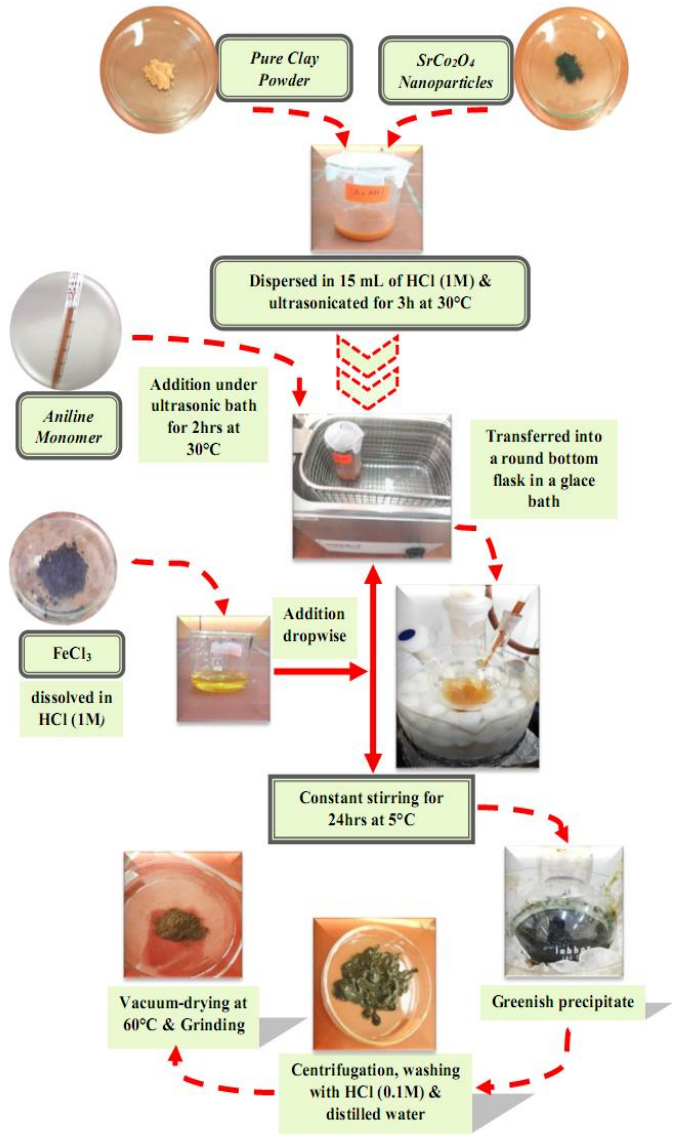

Figure 1.b The scheme of Clay/PANI/$SrCo_2O_4$ nanocomposite synthesis

2.3. Characterization techniques

XRD measurements were carried out with a Bruker D8 Twin-Twin powder diffractometer using a copper anticathode (Cu-Kα, λ = 1.5406 Å), with a step size of 0.002° and scan speed of 2°/min. FT-IR spectra were obtained using Shimadzu 8400 Spectrometer in the wave number range from 400 cm^{-1} to 4000 cm^{-1}. The morphology and elemental analysis were investigated with SEM-EDX using Quanta 250 (with tungsten filament from FEI Company) and Point of zero charge (PZC) of $SrCo_2O_4$ and nanocomposite was measured by pH drift method using an electrolyte solution of NaCl (0.1 M)

2.4. Photocatalytic tests

The photocatalytic activities of as prepared materials were evaluated by degradation of Congo red ($C_{32}H_{22}N_6Na_2O_6S_2$) under UV irradiation in a glass reactor. The suspensions of the dye (7×10^{-4} M) and the photocatalyst (1g/L) contained in test tubes. Initiation of photocatalytic degradation by stirring the suspensions under UV-Visible light (this step lasts 24 hours), in which a tube is removed every 2 hours. After filtration using Whatman filter (0.02µm), the filtrates recovered were analyzed by UV-Visible spectroscopy to determine the degradation rates (figure-2).

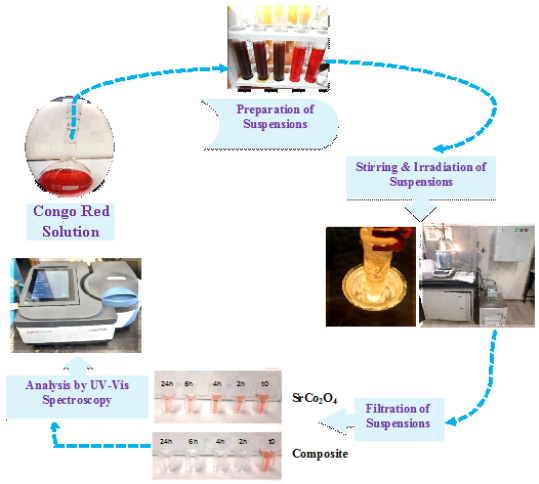

Figure. 2. Photocatalytic activity of $SrCo_2O_4$ and Clay/PANI/$SrCo_2O_4$ nanocomposite.

3. RESULTS AND DISCUSSION

3.1. Characterization

The phase conformation of the Clay/PANI/$SrCo_2O_4$ nanocomposite was determined using powder X-ray diffraction (XRD). The powder XRD of clay, $SrCo_2O_4$, PANI and nanocomposite is illustrated in figure 3. The raw mineral diffractogram showed well-defined reflections at 2θ value of 8.85°, 12.35°, 19.84°, 20.84°, 24.78°, 24.90°, 25.30°, 26.62°, 29.84°, 33.10°, 34.56°, 34.68°, 34.86°, 35.62°, 36.53°, 37.75°, 42.41°, 45.40°, 45.75°, 50.12°, 54.99°, 55.28°, 59.92° and 61.62°, typical characteristic peaks of kaolinite and illite as clay material with non-clay minerals of quartz and small amount of anatase [38-41]. The obtained diffraction patterns of $SrCo_2O_4$ nanoparticle exhibited several peaks located at 2θ= 18.98°, 31.26°, 36.83°, 38.53°, 44.80°, 55.70°, 59.33° and 65.22° correspond to the (111), (220), (311), (222), (400), (422), (511) and (440) crystal planes [42]. All the diffraction peaks obtained for $SrCo_2O_4$ were sharp and well defined, suggesting good crystallization of the sample [43], and confirming the formation of cubic spinel shape $SrCo_2O_4$ nanoparticles with a lattice parameter a=8,109Å and a space group of Fd-3m [44,45]. In addition, No impurities, such as Co_2O_3, CoO or SrO, were detected. Despite its amorphous nature [46], the prepared polyaniline exhibits sharp and wider reflection peaks at 2θ = 9.22°, 14.98°, 20.74°, 25.19°, 25.20°, and 30.09°, which correspond respectively to (001), (011), (020), (200), (121) and (022) crystal planes (JCPDS no 53-1891) [47-50]. XRD patterns of nanocomposite showed a decrease of the reflection peaks of clay and disappearance of those of polyaniline. Whereas, the diffraction peaks of $SrCo_2O_4$ in the nanocomposite become sharper and more apparent. This can be explained by the polymeric intercalation of the clay accompanied by a partial exfoliation and the arrangement of the oxide nanoparticles on its surface. The crystalline grains size of materialsD (nm) is calculated from the full width at half-maximum (FWHM) of the XRD peak β (in rad), using the Debye-Scherrer equation (D=0,9λ/βcosθ) [51,52]. Where: λ is the wavelength of the X-ray radiation ($\lambda_{CuK\alpha}$ = 1.5406 Å), β is the width at mid- at half maximum (FWHM) diffraction peak and θ isthe diffraction angle. The average sizes obtained from the most intense peaks are grouped in table 1.

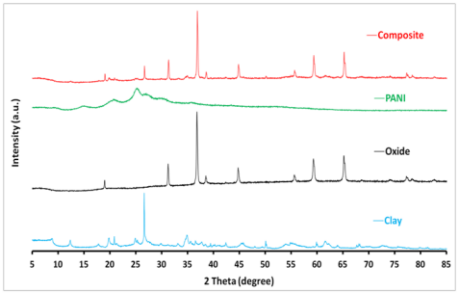

Figure 3. X-ray diffractograms for Clay, $SrCo_2O_4$, PANI and Clay/PANI/$SrCo_2O_4$ nanocomposite.

Table 1. Crystalline sizes of Clay, $SrCo_2O_4$, PANI and Clay/PANI/$SrCo_2O_4$ nanocomposite.

Samples	Clay	$SrCo_2O_4$	PANI	Clay/PANI/$SrCo_2O_4$
D (nm)	60,90	41,88	4,79	35,35

The compositions of raw clay, $SrCo_2O_4$, PANI and formulated nanocomposites were further confirmed by FTIR. The spectra of the samples were obtained by plotting the % of transmittance as a function of wave number in the range of 400 to 4000 cm^{-1} and presented in the figure 4. FTIR spectrum of clay shows firstly two absorption bands near 3620 and 3699 cm^{-1} corresponding to stretching vibration of internal and internal surface OH groups respectively, which are located between the tetrahedral and octahedral surface of the layers confirmed the presence of kaolinite in the raw material [53-55]. The band observed in the spectrum at 1643cm^{-1} corresponds to bending vibrations of the adsorbed water (H-OH) [56-58]. The broad band from 975 cm^{-1} to 1110 cm^{-1} is assigned to the stretching vibration of the Si–O bonds [59]. The frequency vibration 914 cm^{-1} assigned to Al-OH bonds [60]. Another absorption band appears at 528 cm^{-1} and at 443 cm^{-1} due to the symmetric (Si-O-Si) and antisymmetric (Al-O-Si) bending vibration, respectively [61]. The FT-IR spectrum of the prepared $SrCo_2O_4$ nanoparticles by sol-gel process, exhibits two sharp bands occur at 582 cm^{-1} and 663 cm^{-1} related to the stretching vibrations of the metal-oxygen bond in octahedral and tetrahedral sites (Sr-O) and (Co-O), respectively [62,63]. The band at 3407 cm^{-1} corresponds to the stretching mode of O-H group due to the presence of chemisorbed water molecules [64]. The FTIR spectrum of polyaniline (PANI) showed different bands. The stretching vibrations of the N-H bond are visible through the peak present at 3398 cm^{-1} [65]. The two bands appearing at 1558 cm^{-1} and 1475 cm^{-1} correspond to the non-symmetric vibration of carbon–carbon double bond (C=C) of quinoid and benzenoid ring, respectively [66-68], while The broad and strong band observed at 1114 cm^{-1} is characteristic of C-N stretching vibrations [69]. The peak observed at 813 cm^{-1} is related to the aromatic C–H out-of-plane bending vibrations in benzene ring [70]. Finally, the peak at 493 cm^{-1} is associated with the C–H out-of-plane bending vibration [71-73]. According to Figure 4, the spectrum of Clay/PANI/$SrCo_2O_4$ showed peaks at 1234 cm^{-1} and 1290 cm^{-1}, which are the characteristic peaks of polyaniline [74]. The relative intensity of the 1556 cm^{-1} and 1475 cm^{-1} bands indicates the oxidation state of the material [75]. In addition, the peak with wavenumber of 800 cm^{-1} confirms the formation of polymer [76]. The peaks observed in the range of 500–600 cm^{-1} and at 1012 cm^{-1} are due to the presence of clay in the sample [77]. A Strong absorption peaks at 582 cm^{-1} and 663 cm^{-1}, which confirms the presence of $SrCo_2O_4$ spinel nanoparticles.

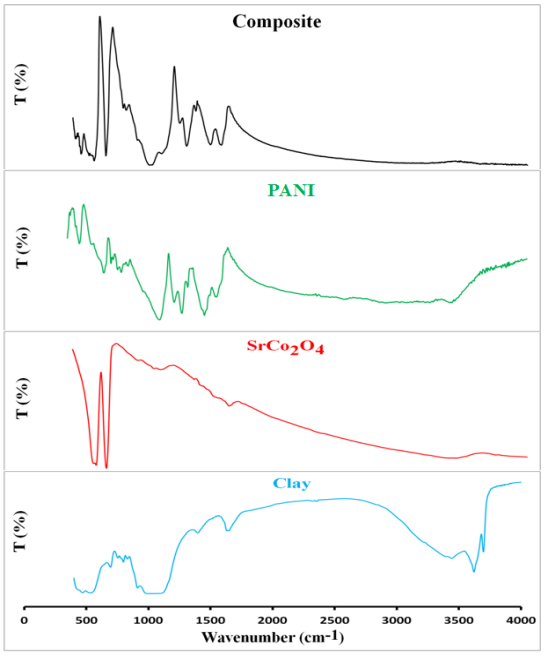

Figure 4. FT-IR absorption spectra of: Clay, $SrCo_2O_4$, PANI and Clay/PANI/$SrCo_2O_4$ nanocomposite.

Scanning electron microscopy (SEM) was carried out to study the morphology of the particles constituting the different materials. Energy-dispersive X-ray spectroscopy (EDAX) was performed to confirm the chemical composition of the prepared nanocomposite. SEM micrographs of the $SrCo_2O_4$ spinel, clay, PANI and nanocomposite with the same magnification and and EDAX image of nanocomposite are shown in the figure 5.

Scanning electron microscopy (SEM) was carried out to study the morphology of the particles constituting the different materials. Energy-dispersive X-ray spectroscopy (EDAX) was performed to confirm the chemical composition of the prepared nanocomposite. SEM micrographs of the $SrCo_2O_4$ spinel, clay, PANI and nanocomposite with the same magnification and and EDAX image of nanocomposite are shown in the figure 5.

The SEM image of $SrCo_2O_4$ shows that the spinel-structured $SrCo_2O_4$ particles synthesized by sol-gel process, merge and transform into massive structures of varied geometries due to the agglomeration phenomenon [78,79]. Scanning electron micrograph presenting the morphology of the clay raw material shows a very fine structure composed of small stacks of flakes of heterogeneous sizes [80,81]. This can be justified by the fragility of the clay made up of a kaolinitic fraction whose particles undergo rupture during treatment. SEM of PANI in figure 5 the figure reveals that the polyaniline (PANI) particles have a flake shape of more or less irregular nanometric sizes. These results are in agreement with the results obtained by M.F. Banjar et al [83]. Several interconnected fibers were observed giving an agglomerated morphology because of the experimental conditions relating to the oxidant/monomer ratio on the one hand and to the temperature on the other hand [84].

The image of as-synthesized nanocomposite reflected the decoration of the clay particles by the polyaniline grains on the one hand and by the $SrCo_2O_4$ particles which appear in the form of nanometric grains with spherical forme, widely distributed on the surface of the nanocomposite.

The EDX spectrum produced in the case of the nanocomposite confirms the in situ synthesis of polyaniline and the integration between the three components to form a ternary Clay/PANI/$SrCo_2O_4$ nanocomposite [85,86].

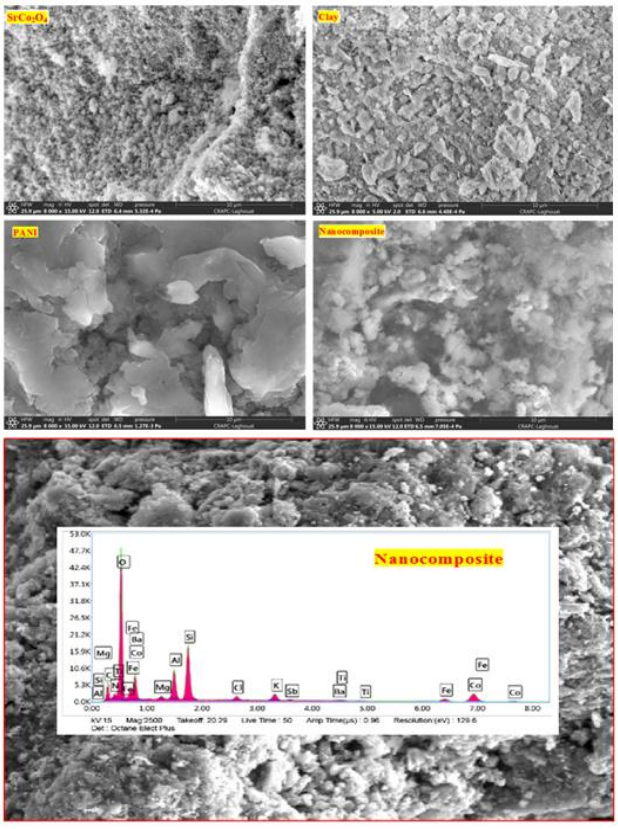

Figure 5. SEM image of $SrCo_2O_4$, raw clay, PANI, nanocomposite and EDX spectrum of the synthetic nanocomposite

pHpzc is one of the main factors in the photocatalytic act because it has a direct relationship with the electrostatic interactions (attraction or repulsion) between the photocatalyst surface and the dye molecules. The value of pHpzc of the $SrCo_2O_4$ and nanocomposite are determined as 6 and 4.5 respectively (Fig. 6). This infers that at pH < pHPZC = 4.5, the nanocomposite surface acquires a positive charge, and it carries a negative charge at pH > pHPZC = 4.5 [87].

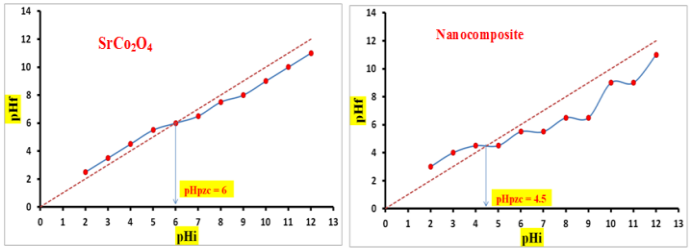

Figure 6. pHPZC determination for $SrCo_2O_4$ and nanocomposite samples.

3.2. Photocatalytic performance:

The photocatalytic performance of the clay/PANI/$SrCo_2O_4$ nanocomposite fabric was evaluated by the photocatalytic degradation of congo red (CR) in an aqueous environment under UV light irradiation. Figure 7 shows the results of the direct photolysis and the photocatalytic degradation of CR on the spinel oxide on the one hand and the nanocomposite on the other hand. It can be clearly seen that the nanocomposite (clay/PANI/$SrCo_2O_4$) exhibited outstanding photocatalytic performance compared to that of pure oxide, further confirming the effectiveness of this material as photocatalyst in water treatment. this improvement in the photocatalytic performance of the oxide is due to its immobilization on materials (intercalated clay), because the support offers the photocatalyst a higher surface area and reduces the agglomeration of its nanoparticles [88,89].

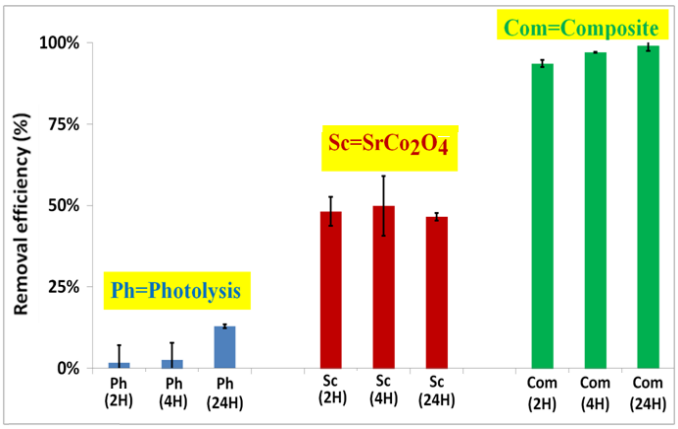

Figure 7. Photolysis and degradation rate (%) of CR on $SrCo_2O_4$ and Clay/PANI/$SrCo_2O_4$.

The possible photocatalytic reaction process can be proposed as follows:

$$\textit{UV light irradiation}: \quad Nanocomposite \rightarrow h^+_{VB} + e^-_{CB} \tag{1}$$

$$\textit{Adsorbed } O_2: \quad O_{2(ads)} + e^- \rightarrow \cdot O_2^- \tag{2}$$

$$\textit{Adsorbed } H_2O: \quad \begin{cases} \cdot O_2^- + H_2O \rightarrow \cdot OH + HO_2^- \\ h^+ + H_2O \rightarrow \cdot OH + H^+ \end{cases} \tag{3}$$

$$\textit{Adsorbed CR molecules}: \quad \begin{cases} \cdot OH + CR_{ads} \rightarrow CO_2 + H_2O \\ \cdot O_2^- + CR_{ads} \rightarrow CO_2 + H_2O \\ h^+ + CR_{ads} \rightarrow CO_2 + H_2O \end{cases} \tag{4}$$

Based on the results of this experimental research, the photocatalytic mechanism of Clay/PANI/$SrCo_2O_4$ photocatalyst during CR degradation under UV light irradiation is depicted in Figure 8.

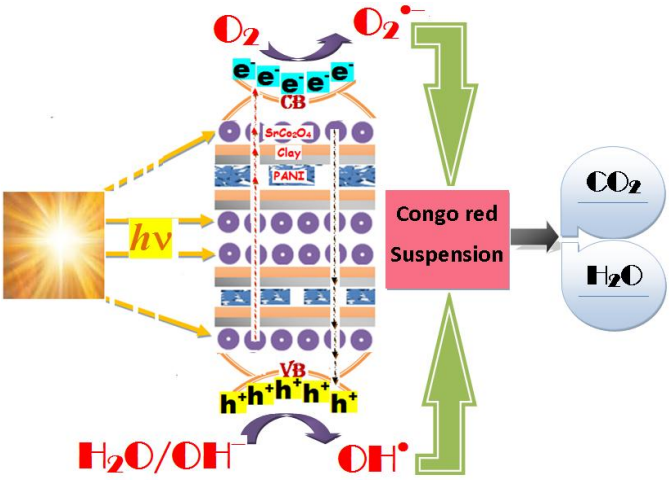

Figure 8. Schematic illustration of Clay/PANI/$SrCo_2O_4$ nanocomposite photocatalytic mechanism.

CONCLUSIONS

Nanocomposites are combinations of several materials with a certain affinity to constitute stable materials and often complementary properties. In this work, a new cobalt-based spinel material was prepared by sol-gel process and then mobilized on a clay matrix modified by polyaniline prepared in situ. The pure oxide and the nanocomposite were characterized by different techniques and then tested as photocatalysts under visible light by the degradation of the Congo red dye. The results of the photocatalytic test show a good improvement in the photocatalytic activity of the oxide following its mobilization.

REFERENCES

1. Y. Zhang *et al*., *Chemosphere* **341**,140038,(2023).
2. R. Gusain *et al*., *Adv. Colloid Interface Sci.* **272**,102009,(2019).
3. P. O. Oladoye *et al*., *Groundw. Sustain. Dev*. **19**, 100844,(2022).
4. K. Alau *et al*., *Arch. Appl. Sci.* Res. **2**, 456,(2010).
5. V. K. Gupta *et al*., *Global. J. Environ. Sci. Manage.* **1**,71,(2015).
6. A. Seidmohammadi *et al*., *Arch. Hyg. Sci.* **4**, 217,(2025).
7. V. Chandanshive *et al*., *Chemosphere.* **252**,126513,(2020).
8. H. Ramezanalizadeh and E. Rafiee. *Sci. Semicond. Process.* **113**, 105055,(2020).
9. A. S. Kadari *et al*., *Inorg. Chem. Commu.* **142**,109626,(2022).
10. K. Litefti *et al*., *Sci. Rep.* **9**,16530,(2019).
11. N.A. Alamrani *et al., Adsorpt. Sci. Technol.* **2021**,1,(2021).
12. P. Arsana *et al*., *J. Appl. Sci.* **12**,1809(2012).
13. Y. Choi *et al., Water*. **9**,409(2017).
14. B. Lellis *et al., Biotechnol. Res. Innov.* **3**,275,(2019).
15. N. N. Mahamuni and Y. G. Adewuyi, *Ultrason. Sonochem.* **17**,990,(2010).
16. J. de Koning *et al., Desalination*, **218**,92,(2008).
17. S. S. Srinivasan *et al., J. Nanomaterials*. 2006,1,(2006).
18. P. Chen *et al*., *EcoMat.* **2**,12047(2020).
19. E. Kowalska et al., Chapter 16. In book: Visible Light-Active Photocatalysis,2018.
20. N. Shaheen *et al., Phys. B: Condens. Matter.* **580**,411820,(2020).
21. J. Chen *et al., Mater. Lett*. **220**,66,(2018).
22. M. Kaikhosravi *et al., Mater. Chem. Phys.* **170**,62,(2016).
23. Y. Wan *et al, J. Environ. Chem. Eng.* 6,6079, (2018).
24. A. Gouasmia *et al., Inorg. Chem. Commun.* **145**,110066,(2022).
25. R. Rahmatolahzadeh *et al., J. Inorg. Organomet. Polym. Mater.* **27**,313,(2017).
26. M. H. Habibi and P. Bagheri, *J. Mater. Sci: mater. electron*. **28**,289,(2017).
27. A.A. Yadav *et al., Ultrason. Sonochem*. **58**,104663,(2019).
28. E.G. Garrido Ramírez *et al., Appl. Clay Sci.* **47**,182,(2010).
29. J. Herney-Ramirez *et al, Appl. Catal. B.* **98**,10,(2010).
30. C. Chuaicham *et al., Separations*. **10**,77,(2023).
31. C. Li *et al., Adv. Powder Technol.* **31**,1241,(2020).
32. Z. Sun *et al., J. Colloid Interface Sci*. **565**,11,(2020).
33. Y. Tan *et al., J. Colloid Interface Sci.* **564**,143, (2020).
34. B. Demir *et al., RSC Adv.* **3**,7513,(2013).
35. L. Jankovic *et al., Appl. Clay Sci.* **204**,105989, (2021).
36. R.K. Kukkadapu and S.A. *Clays. Clay. Miner.* **43**,318, (1995).
37. N. G. Duran *et al., Mater. Chem. Phys*. **118**,93,(2009).
38. S. Biswas *et al., Clay. Int. J. Polymer. Sci.* **2017**,1,(2017).
39. M G F. Rodrigues., *Ceramica*, **49**,146, (2003).
40. E. Gunister *et al, Carbohydr. Polym*. **67**,358, (2007).
41. H H. El-Maghrabi and S. Mikhail, *J. environ. Earth. sci*. **4**,38, (2014).
42. K. Tamil Thendral *et al., Mat. Lett*. **349**,134720, (2023).
43. H. Chen *et al., Nanoscale. Adv*. **2**,3263, (2020).
44. R. K. Sharma *et al., Mater. Today.* **4**,5667, (2017).
45. A. Kruk *et al., Physica B: Physics of Condensed Matter*. **596**,412402, (2020).
46. M. Porramezan and H. Eisazadeh, *Composites: Part B*. **42**,1980, (2011).
47. Y. Li *et al., Polym. Polym. Compos*. **27**,76, (2019).
48. L R. Vargas *et al., J. Aerosp. Technol. Manag.* **9**,29, (2017).
49. K T. Vadiraj and S.L. Belagali, J. Appl. Chem. 8,53, (2015).
50. W. Lin *et al, RSC Adv*, **4**,39508,(2014).
51. B.D. Cullity and S.R. Stock, Elements of X-Ray Diffraction, Prentice Hall, (2001).
52. D W. Fu *et al, Adv. Mater.* **23**,5658, (2011).
53. A. Tironi *et al., Constr. Build. Mater*. **28**,276, (2012).
54. J. Madejova., *Vib. Spectrosc*. **31**,1, (2003).
55. O. Ombaka, *Afr. J. Environ. Sci. Technol*. **10**,415, (2016).
56. H. Cheng *et al., Spectrochimica Acta Part A*. **77**,1014, (2010).
57. R. L. Frost *et al., Spectrochimica Acta Part A*. **57**,603, (2001).
58. D. Liu *et al., Minerals*. **12**,54 (2022).
59. S. Arellano-Cardenas *et al., Clays. Clay. Miner.* **60**,153, (2012).
60. A. G. Olaremu., *J. Minerals. Mater. Charac. Eng.***3**,353,(2015).
61 A. Er-ramly and A. Ider., *Am. J. Nano. Res. Appl*. **4**,17, (2016).
62. S. Jayasubramaniyan *et al., J Mater Sci: Mater Electron.* **29**,21194, (2018**).**
63 M. Kaikhosravi *et al, Mater. Chem. Phys.* **170**,62, (2016).
64. X. Xiao *et al, Sci. Reports*. **8**,7571, (2018).
65. A N J. Al-Daghman *et al, Adv. Phys. Theor. Appl.* **47**,18 (2015).
66. P. Kolhar *et al., Nanomaterials.* **13**,2223,(2023).
67. W. Shao *et al., Materials.* **5**,1811, (2012).
68. Q. MO *et al., J. Ceram. Soc. Jpn.* **128**,135, (2020).
69. H. Gu *et al., Polymer*. **143**,324, (2018).
70. E. Akbarinezhad *et al., Prog. Org. Coat*. **70**,39,(2011).
71. M. Afzali *et al., Microchem. J.* **145**,373(2019).
72. M. Ayad *et al., Chem. Eng. J.* **217**,460, (2013).
73. D M. Jundale *et al., J. Mater. Sci. Mater. Electron.* **24**,3526, (2013).
74. B S. Singu *et al., J. Electrochem. Soc.* **159**,6, (2012).
75. D. Priyanka and K. S. Venkatesh., *Int. J. Eng. Res. Appl*. **5**,53, (2015).
76. M. Porramezan and H. Eisazadeh, *Composites: Part B* **42**,1980,(2011).
77. H. Soltani *et al., J. Inorg. Organomet. Polym*. **29**, 841, (2019).
78. L. Chandra *et al., ACS Omega* **7**,4859, (2022).
79. Z. Mousavi *et al., Sci. Rep*. **6**,20071, (2016).
80. M. Valášková *et al., Appl. Clay Sci.* **35**,108, (2007).
81. R. Dewi *et al., J. Phys: Conf. Series.* **1116**,042010, (2018).
82. A Nugroho *et al., Sci. Technol. Publ. Lda*, 48-53,(2020).
83. M F. Banjar *et al., Polymers* **15**,4565, (2023).
84. R. Idrees *et al., Heliyon*. (2024).
85. R.B. Asamoah *et al., Materials.* **13**,3793, (2020).
86. M R. Abukhadra *et al., int. j. environ. anal. Chem*. **104**,879,(2024).
87. M. R. Elamin *et al., Inorg. Chem. Commun.* **159**,111840, (2024).
88. A. Joseph and A. Vijayanandan., *Inorganica. Chimica. Acta*. **545**,121284, (2023).
89. H. S. Zakria *et al., RSC Adv*. **11**,6985,(2021).